JOURNAL OF MATERIALS SCIENCE 26 (1991) 583–587

The activation energies of the crystallization of amorphous $Ni_{81}P_{19}$ alloy films

T. IKARI, M. IZAKI*, T. FUKUMORI*, K. FUTAGAMI
*Department of Electronics and *Department of Applied Physics, Miyazaki University, 1-1 Gakuen Kibanadai, Miyazaki 889-21, Japan*

In situ transmission electron microscopic observations were carried out to study the crystal growth kinetics of amorphous $Ni_{81}P_{19}$ alloy films prepared by vacuum deposition. In the first stage of crystal growth a metastable Ni_3P phase with hexagonal symmetry appeared. The growth rates were independent of time at a given annealing temperature. The activation energies along [1 0 0] and [1 1 0] directions were estimated to be 3.12 eV for the 55 nm thick and 3.22 eV for 20 nm thick film samples. Similar measurements for the stable and the metastable phases of thin foil samples were also carried out. The smaller activation energies for the foil samples than the film samples are explained by assuming that the compositional requirement at the crystalline–amorphous interface and the jumping of atoms to the crystal sites occur in series.

1. Introduction

Amorphous metallic alloy is well known as a new material which has a high magnetic permeability and excellent resistance to corrosion. Since these technological applicabilities of amorphous alloys deteriorate drastically on crystallization, the crystallization kinetics have been extensively studied. Further attention has been paid to the appearance of metastable crystalline phases during crystallization of the amorphous materials. This is because such metastable phases could not be obtained by the usual crystal growth technique.

The crystallization of an amorphous Ni–P alloy was studied first with a transmission electron microscope (TEM) by Bagley and Turnbull [1]. Although the Ni–P alloy is the simplest and most typical metal–metalloid system, its crystallization process is rather complex and the crystal growth kinetics has not been well understood. In the binary alloy phase diagram of the Ni–P system [2], the eutectic reaction occurs at a temperature of 880 °C and a composition of 19 at % P. When the amorphous alloy has a composition near this eutectic point, a two-phase mixture of nickel and Ni_3P may appear by annealing. This stable Ni_3P phase has a body-centred tetragonal (bct) crystal structure with lattice constants of $a = 0.8954$ nm and $c = 0.4386$ nm [3].

Three metastable hexagonal phases were observed by TEM measurements in the crystallization process of amorphous Ni–P electrically or chemically deposited alloys with 14 to 25 at % P compositions [4]. They are identified as α_1 ($a = 0.672$, $c = 0.952$ nm), α_2 ($a = 0.672$, $c = 1.428$ nm) and α_3 ($a = 0.672$, $c = 3.808$ nm). Since the parameters a of these metastable phases are the same but c values differ in the ratio of 2:3:8, these form a family of hexagonal polytypes. However, no investigations have so far been carried out on the crystal growth kinetics of these metastable phases.

In this paper, we report on the results of *in situ* TEM observation of the crystallization of amorphous $Ni_{81}P_{19}$ vacuum-evaporated thin films by isothermal annealing. The activation energy of the crystal growth rate is measured for the metastable phase and the crystal growth kinetics will be discussed. Similar measurements on foil samples with the same composition were also carried out for comparison.

2. Experimental procedure

The thin film samples were prepared by vacuum evaporation of amorphous $Ni_{81}P_{19}$ ribbon on to glass microscope slides held by a large heat sink made of a copper metal block. Splat-quenched ribbon (Japan Amorphous Metal Co., Metglas MBF60) was used as an evaporation source. The temperature of the evaporation source was 1300 to 1400 °C and the pressure was of the order of less than 10^{-3} Pa. The deposited film thicknesses were 20 to 50 nm and the deposition rate was typically 20 nm min^{-1}. The evaporated films were uniform and the phosphorus composition was determined by an electron probe X-ray microanalyser as 19 at %. Selected-area electron diffraction (SAD) patterns of the thin films always showed halos. These experimental results indicate that the evaporated thin film is an amorphous one whose composition is the same as that of the $Ni_{81}P_{19}$ ribbon. Similar uniform amorphous films were also prepared by flash evaporation. In this case, however, films of sufficient thickness could not be obtained because of degradation of the tungsten heating wires.

Thin foil samples were prepared from amorphous $Ni_{81}P_{19}$ ribbon with a thickness of 40 μm. Polishing was done with a jet electrolyte of

0022–2461/91 $03.00 + .12 © *1991 Chapman and Hall Ltd.*

$CH_3COOH(7):HClO_4(3)$ solution kept at $-10\,^{\circ}C$ to control the polishing rate accurately. Since the jets were operated from both sides of the specimen, the initially parallel-sided specimen became dish-shaped and finally perforated. The specimen then had a wedge shape around the hole. Bright-field images of the foil showed that quenched-in nuclei of diameter about 2 to 3 μm were involved. These were identified by SAD as stable b c t Ni_3P crystals. Insufficient quenching from the melt to obtain the amorphous ribbon may cause these inclusions.

In situ isothermal annealing was carried out by using a heating stage in the objective chamber of the TEM (Hitachi, H-800MU). The acceleration voltage was set at 200 kV. To obtain the annealing temperature dependence of the crystal growth rate, the temperature of the heating stage was changed step-wise and observations were carried out at each temperature. TEM images were continuously recorded on film at time intervals of about 1 min after the nucleation occurred. The time intervals depended on the annealing temperature. The crystallized phase grew into the amorphous matrix with time. The crystal growth rate was therefore estimated by measuring the distances between the moving fronts of the crystalline–amorphous interfaces of successive images.

Figure 1 Bright-field TEM image of film evaporated at 370 °C for 10 min. The thickness was 55 nm. Spherulitic and rectangular metastable crystals are observed.

3. Results and discussion

3.1. Crystallization reactions

Fig. 1 shows a bright-field TEM image of an evaporated thin film of 55 nm thickness annealed at 370 °C for 10 min after the nucleation occurred. Spherulitic and rectangular phases are observed. A typical SAD pattern of the spherulitic phase is shown in Fig. 2a. Analysis of the SAD patterns indicates that the spherulitic phase is a hexagonal metastable Ni_3P phase with a lattice constant of $a = 0.656$ nm. The incident electron beam was set along the crystallographic [0 0 1] axis and the (1 1 0) reflection is indicated by an arrow in the figure. The SAD pattern for the rectangular phase shows that this phase is also metastable Ni_3P, but in this case, the crystallographic [0 0 1] axis is in the film plane and is along the shorter side of the rectangular crystals. The lattice constant c could be determined as 1.392 nm. This shows that our metastable phase is the α_2 metastable phase reported by Kuo *et al.* [4]. The α_1 and α_3 phases could not be observed in the present investigations. For the film of 20 nm thickness, only the spherulitic crystals were observed.

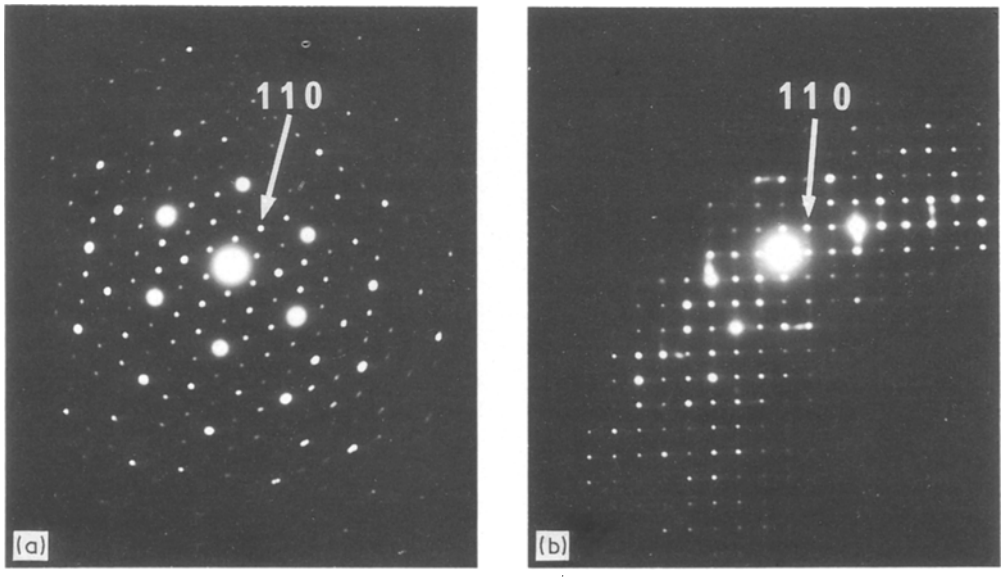

Figure 2 SAD patterns of (a) metastable and (b) stable Ni_3P crystals. The incident electron beam is along the [0 0 1] axis. The reflections for the (1 1 0) plane are indicated by arrows.

During isothermal annealing, the metastable phase grows along the radial direction of the spherulitic crystal. The growth length was measured by the movement of the crystalline–amorphous interface on the photographs. Since the crystals grow rapidly perpendicular to the [0 0 1] axis and collide with each other in the case of the rectangular crystals, only the growth length along the [0 0 1] axis could be measured.

When the temperature of the thin film sample was raised to 520 °C, the metastable spherulitic crystals transform to stable Ni_3P crystals. A typical SAD pattern of a transformed stable Ni_3P crystal is shown in Fig. 2b. Fourfold symmetry is clearly observed. The lattice parameters of the stable Ni_3P crystals are estimated as $a = 0.907$ nm and $c = 0.438$ nm from SAD patterns of different crystal orientations. These agree with those reported by Kuo *et al.* [4] within the experimental error. No systematic correlation of the crystal orientations between the metastable and the transformed stable phases could be observed.

We also investigated the crystal growth kinetics of foil samples prepared from the $Ni_{81}P_{19}$ amorphous ribbon. A typical bright-field TEM image of a foil sample is shown in Fig. 3. The annealing temperature was 290 °C. The crystal phase was identified as the metastable hexagonal Ni_3P phase from its SAD pattern. The [1 1 0] direction is perpendicular to the edge of the foil and the [0 0 1] axis is almost perpendicular to the foil plane. The metastable phase grows from the edge of the sample by annealing. Small precipitates of diameter less than 5 nm appear from the initial stage of annealing and were identified as crystalline nickel particles from the SAD patterns. The dark fringes in the metastable phase are considered to be grain boundaries which appear in the thicker part of the sample. Metastable phases growing from the two surfaces of the foil collide with each other and may form these grain boundaries.

The metastable phase in the foil sample transforms to the stable Ni_3P phase when the annealing temperature exceeds 430 °C, as in the case of thin film samples. Furthermore, in the thicker part of the foil sample, growth of stable Ni_3P phases could be observed below 430 °C. Quenched-in nuclei of stable Ni_3P, which were observed in the bright-field TEM images, act as seeds for the crystallization.

3.2. Crystal growth rate of the Ni_3P phase

The measured crystal growth length as a function of the annealing time is shown in Fig. 4 for typical cases. The data for the metastable phases of film and foil samples are indicated by (a) and (c), respectively. The data in plot (b) were taken from measurements for the stable phase in the foil samples. All the experimental data fall on straight lines, and this fact indicates that the crystal growth rate is constant at a given annealing temperature. This is linear-growth crystallization as in the case of $Fe_{75}B_{25}$ [5] or $(NiPd)_{41}P_{18}$ [6] amorphous alloys. This kind of transformation from amorphous to crystalline phases involves only atomic jumps across the crystallization front without any change in composition, and does not require any long-range diffusion [7].

The crystal growth rates were estimated from the slopes of the straight lines in Fig. 4 and are shown in Fig. 5 as a function of the inverse temperature. The uncertainty of the growth-rate estimation is taking into account by drawing error bars for each datum point in Fig. 5. The crystal growth direction is designated by open and solid circles for the [1 1 0] and [1 0 0] axes, respectively. The growth rates along the [0 0 1] axis, indicated by triangles, were obtained only for thin film samples of 55 nm thickness, where the [0 0 1] axis is in the film plane.

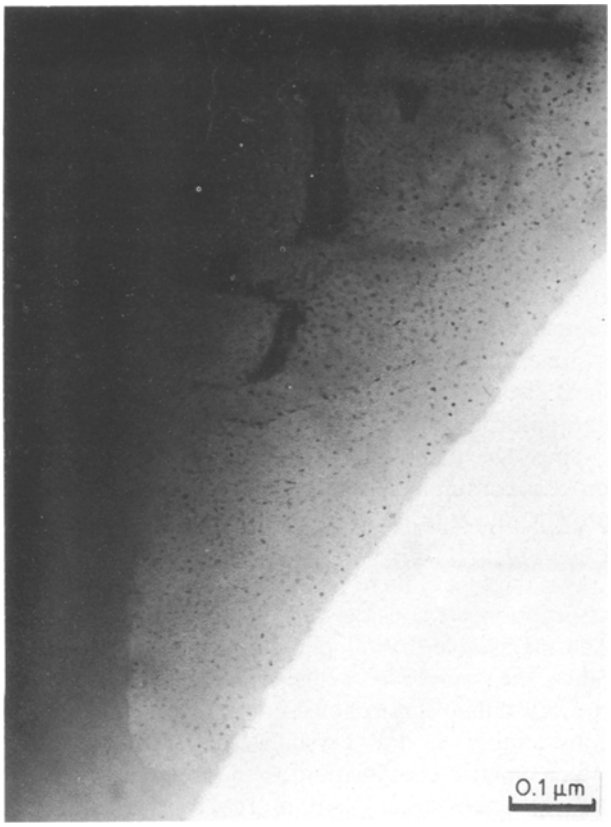

Figure 3 Bright-field TEM image of the metastable phase in a foil sample annealed at 290 °C. The small precipitates are nickel crystals of diameter less than 5 nm. The [1 1 0] direction is perpendicular to the edge of the film.

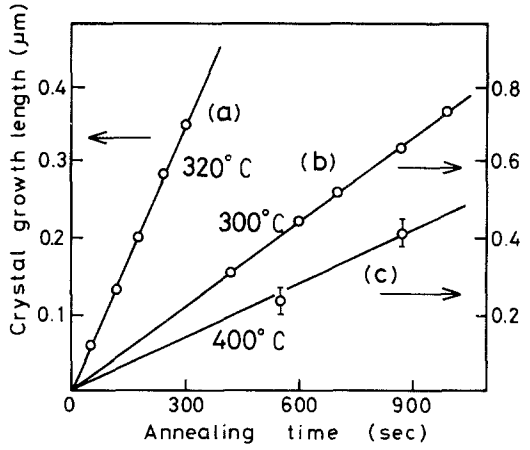

Figure 4 Crystal growth length as a function of isothermal annealing time for (a) the metastable phase in the foil, (b) the stable phase in the foil and (c) the metastable phase in the film. The growth directions are along the [1 1 0] axis.

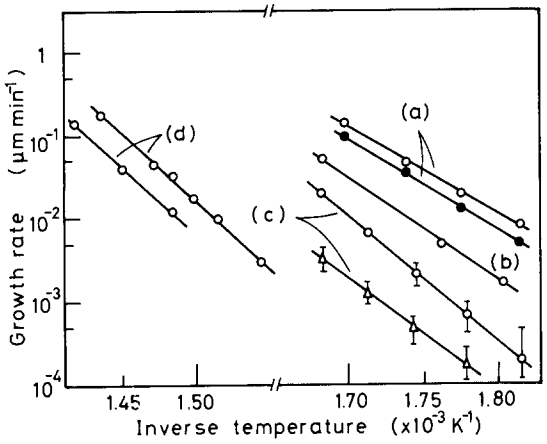

Figure 5 Crystal growth rate as a function of temperature for (a) stable and (b) metastable phases in foil, and for the metastable phase in films of thickness (c) 55 nm and (d) 20 nm. The directions of growth are (○) [1 1 0], (●) [1 0 0] and (△) [0 0 1].

Since the length of the growing crystals exhibits a linear time dependence at all temperatures as shown in Fig. 4, the growth rate V of crystals can be expressed by the equation [7]

$$V = \nu\delta\exp(-E_a/kT) \quad (1)$$

where E_a is the activation energy for growth, ν is the characteristic frequency and δ the interface width. The change in the chemical free energy accompanying crystallization was assumed to be large compared with the measured temperatures and E_a and was neglected in Equation 1. The observed straight lines in Fig. 5 show that the growth rates are well explained by Equation 1. The estimated activation energies are listed in Table I. For the metastable phase observed in the thin film sample, E_a along the [1 1 0] and [1 0 0] axes is 3.12 to 3.22 eV and slightly depends on the film thickness. For the foil samples it is 2.28 eV. The activation energy of the metastable phase along the [0 0 1] axis is estimated to be 2.8 eV. Due to the scatter of the data for the [0 0 1] direction, the growth rate is somewhat uncertain. However, it would be reasonable to consider that E_a along the [0 0 1] axis is almost the same as that along the [1 1 0] and [1 0 0] axes.

For the stable Ni_3P phase of the b c t structure, E_a along the [1 1 0] axis is 2.50 eV. No observation along the [0 0 1] axis could be carried out, since the [0 0 1] axis of the stable phase is always perpendicular to the surface of the foil plane. As stated earlier, the crystal growth length was proportional to the annealing time. A similar time-independent crystal growth rate has been observed for b c t Fe_3B crystals grown from $Fe_{75}B_{25}$ amorphous alloy [5]. The observed activation energy was then about 2.0 eV and had a weak temperature dependence. The concept of multiple processes of temperature-independent activation energies could explain these experimental results. In the present case of Ni_3P, no such complex mechanisms would be necessary to understand the crystal growth kinetics.

When a compositional requirement for the formation of Ni_3P occurs in $Ni_{81}P_{19}$ alloy, the long-range diffusion of phosphorus atoms plays a role in crystal growth [7]. However, in our case for the foil samples,

TABLE I The activation energies for crystallization of Ni_3P phases (estimated from the slopes in Fig. 5)

Sample	Thickness (nm)	Direction	E_a (eV)
Thin film	55	[1 1 0] and [1 0 0]	3.12
(metastable		[0 0 1]	2.8
phase)	20	[1 1 0] and [1 0 0]	3.22
Foil (metastable phase)		[1 1 0] and [1 0 0]	2.28
Foil (stable phase)		[1 1 0]	2.50

this long-range diffusion is not likely to have occurred. This is because the crystal growth rate is time-independent at each annealing temperature. The deficit of the phosphorus atoms forming an Ni_3P phase may be partly compensated by the deficit of nickel atoms due to precipitation in the matrix. A linear dependence of growth length on time would therefore be expected as shown in Fig. 4.

The activation energies of the metastable phase for the thin film samples are larger than for foil samples (Table I). It has been argued that the crystallization processes of Ni–P electrolyte-deposited film depend on the thickness of the sample [8]. In the thin film samples, the crystal growth may be partly limited by the surface boundaries. Since the crystal growth rate was time-independent, long-range diffusion of phosphorus atoms may not contribute to the crystal growth kinetics, as discussed above. We consider here two processes for the crystal growth kinetics.

The first process is considered to be as follows. Since the amorphous phase has a different composition from that of Ni_3P, concentration fluctuations or off-stoichiometry exist at the interface. Therefore, in order to grow the metastable phase, diffusion of the constituent atoms should occur to form the stoichiometric composition. If long-range diffusion of phosphorus atoms is not likely to occur, release of the nickel atoms from the boundary would take place.

The second process is the usual jumping of constituent atoms from the crystalline–amorphous interface to the crystal sites of the hexagonal lattice. We further assume that these two processes operate in series to form the metastable phase of Ni_3P at the crystalline–amorphous interfaces.

Since the first process is followed by the second process continuously, it is assumed that the crystal growth rate still has a temperature dependence as in Equation 1. In this case, the observed activation energy is the sum of these two processes. Based upon this assumption, we consider first the case of foil samples. The metastable crystal phase grows from the edge. Since the sample is wedge-shaped, the volume of the crystalline–amorphous interface layer increases considerably as the crystallization proceeds. The stoichiometric composition at the interface is therefore attained easier than in the case of the thin film samples. Furthermore, the existence of nickel precipitates (Fig. 3) results in a decrease of the off-stoichiometry. In this case, the activation energy of the crystal growth rate is determined by the jumping of

atoms across the interface layer, i.e. only by the second process. It was 2.28 eV for the metastable phase.

In the case of thin film samples, a change of the composition to stoichiometry should occur prior to the jumping of constituent atoms. This is because the film is uniform and there are no precipitates at the first stage of crystallization. The observed activation energies of 3.12 or 3.22 eV are therefore larger than that of the foil samples. The thinner the film thickness, the larger the activation energy: E_a for the 20 nm thick sample is slightly larger than for the 55 nm thick samples.

Similar arguments can be used for the stable phase of Ni_3P. The observed activation energy of 2.50 eV is due to the jumping of atoms to the crystal sites in the bct structure. It is reasonable to consider that the crystal growth rate may have its highest value for crystallization from the stoichiometric amorphous phase [5]. According to the above discussion, non-stoichiometry at the interface was more significant in the film sample than in the foil samples. This leads to a decrease of crystal growth rate for thin film samples, as shown in Fig. 5.

We have carried out measurements of the crystal growth rate of metastable and stable Ni_3P crystals derived from the amorphous phase. Future studies of the phase transformation from the metastable to the stable phase at higher annealing temperatures may give us further insight into the crystal growth kinetics from the amorphous phase. In addition to the study of the crystal–crystal phase transformation, an estimation of the nucleation rate in isothermal annealing should also be done.

4. Conclusions

Crystallization of the metastable and stable Ni_3P phases from an $Ni_{81}P_{19}$ amorphous matrix was studied by isothermal annealing under the transmission electron microscope. The samples were made by vacuum evaporation and splat-quenching of the melt. The hexagonal metastable phase grows as spherulites and rectangular crystals in the thin film samples. They are determined as α_2 hexagonal phase. Isothermal annealing study shows that the crystal growth rate is time-independent at each annealing temperature for both metastable and stable phases. This linear dependence indicates that the long-range diffusion of phosphorus atoms is not likely to occur. For the thin film samples, the activation energies of the metastable phase are 3.12 and 3.22 eV for 55 and 20 nm thick samples, respectively. The activation energies of the foil samples are smaller than those of the thin film samples. This is explained by assuming that a compositional change near the crystalline–amorphous interface occurs in the thin film samples. This process of compositional change is followed continuously by the jumping of the constituent atoms. The precipitation of nickel particles in the foil samples results in a reduction of the activation energy. The observed activation energy for the atomic jumping is 2.28 eV for the metastable and 2.50 eV for the stable crystal phase.

Acknowledgements

Thanks are due to Professor Y. Akashi and Mr T. Matsuo for valuable discussions.

References

1. B. G. BAGLEY and D. TURNBULL, *J. Appl. Phys.* **39** (1968) 5681.
2. T. B. MASSALSKI, J. L. MURRAY, L. H. BENNETT and H. BAKER (eds), in "Binary Alloy Phase Diagram" (American Society for Metals, New York, 1986) p. 1739.
3. E. VAFAEI-MAKHSOOS, *J. Appl. Phys.* **51** (1980) 6366.
4. K. H. KUO, Y. K. WU, J. Z. LIANG and Z. H. LAI, *Phil. Mag. A* **51** (1985) 205.
5. Y. KATAO, M. KIRITANI and F. H. FUJITA, *J. Mater. Sci.* **19** (1984) 3375.
6. P. G. BOSWELL, *Scripta Metall.* **11** (1977) 701.
7. G. K. DEY and S. BANERJEE, *Mater. Sci. Engng.* **76** (1985) 127.
8. R. J. KEYSE and C. HAMMOND, *Mater. Sci. Technol.* **3** (1987) 963.

Received 24 July
and accepted 22 November 1989